

# Probing the heavy Higgs boson production and decay $H_0$ of the Bestest Little Higgs Model at the LHC and the FCC-hh

E. Cruz-Albaro<sup>\*,1</sup> A. Gutiérrez-Rodríguez<sup>†,1</sup> D. Espinosa-Gómez

<sup>‡,2</sup> T. Cisneros-Pérez <sup>§,3</sup> and F. Ramírez-Zavaleta <sup>¶2</sup>

<sup>1</sup>*Facultad de Física, Universidad Autónoma de Zacatecas*

*Apartado Postal C-580, 98060 Zacatecas, México.*

<sup>2</sup>*Facultad de Ciencias Físico Matemáticas,*

*Universidad Michoacana de San Nicolás de Hidalgo*

*Avenida Francisco, J. Mújica S/N, 58060, Morelia, Michoacán, México.*

<sup>3</sup>*Unidad Académica de Ciencias Químicas, Universidad Autónoma de Zacatecas*

*Apartado Postal C-585, 98060 Zacatecas, México.*

(Dated: March 14, 2024)

## Abstract

In the Bestest Little Higgs Model (BLHM) scenario, we analyze the branching ratios and production cross-section of the heavy Higgs boson  $H_0$ . The analysis is performed at the tree level and the one-loop level. In addition, we present results of the possible production of the heavy Higgs boson  $H_0$  via gluon fusion for the center-of-mass energies and the integrated luminosities of the LHC, HE-LHC, HL-LHC, and FCC-hh. Our results show a very optimistic scenario for studying the  $H_0$  scalar predicted by the BLHM and for the energies and luminosities of current and future hadron colliders.

PACS numbers: 14.80.Cp, 13.87.Ce

Keywords: Non-Standard-Model Higgs bosons, Production.

---

\* elicruzalbaro88@gmail.com

† alexgu@fisica.uaz.edu.mx

‡ david.espinosa@umich.mx

§ tzihue@gmail.com

¶ feryuphy@yahoo.com.mx

## I. INTRODUCTION

There are convincing theoretical arguments and a wide range of experimental facts that motivate the need for new physics beyond the Standard Model (SM), such as the hierarchy problem, the strong CP problem, the baryon asymmetry of the universe, the existence of dark matter, the fine-tuning of the Higgs boson mass, the origin of fermionic families, etc.. Most of the solutions to these problems require new interactions and new particles, such as supersymmetric partners, heavy Higgs bosons, dark photons, axions, right-handed neutrinos, and monopoles, among other things.

Many of the proposed new physics models contain an extended Higgs sector, among which the BLHM [1–7] is one of the viable options because it provides an exciting way to address the hierarchy problem without resorting to fine-tuning. In addition, it solves some issues that are present in the great majority of the other Little Higgs models (The Littlest Higgs Model [8], A Littlest Higgs Model with custodial  $SU(2)$  symmetry [9], The Little Higgs Model [10], The Little Higgs Model and custodial  $SU(2)$  [11], The Simplest Little Higgs Model [12]), such as the problem of dangerous singlets [13], a pathology where collective symmetry breaking does not suppress quadratically divergent corrections to the Higgs boson mass; and strong constraints from precision electroweak observables [14, 15] in the gauge sector. Instead, the BLHM generates a viable Higgs quartic coupling where the real singlet  $\sigma$  is no longer a dangerous singlet; that is, it no longer develops a divergent tadpole from radiative corrections [1]. On the other hand, a custodial  $SU(2)$  symmetry [16] and disassociation in the masses of the new quarks and heavy gauge bosons are implemented in the BLHM, thus avoiding the constraints from precision measurements.

The disassociation in the masses of the partners of fermions ( $T$ ,  $B$ ,  $T_5$ ,  $T_6$ ,  $T^{2/3}$ ,  $T^{5/3}$ ) and gauge bosons ( $Z'$ ,  $W'^{\pm}$ ) is achieved by incorporating two independent symmetry-breaking scales,  $f$  and  $F$  with  $F > f$ . This leads to new quarks with masses proportional only to the  $f$  scale, while the new gauge bosons acquire masses proportional to the combination of the  $f$  and  $F$  scales. Since the new quarks are now lighter than the new gauge bosons, fine-tuning in the top sector and electroweak precision constraints in the gauge sector are avoided. In the scalar sector, neutral and charged physical scalar fields also arise:  $h_0$ ,  $H_0$ ,  $A_0$ ,  $\phi^0$ ,  $\eta^0$ ,  $H^{\pm}$ ,  $\phi^{\pm}$  and  $\eta^{\pm}$ . The  $h_0$  state is assumed to be light ( $\approx 125$  GeV), similar to the Higgs of the SM, while the rest of the scalars are allowed to vary their masses.

In this paper, we explore the production of the heavy Higgs boson  $H_0$  of the BLHM at current and future colliders such as the Large Hadron Collider (LHC) and the Future Circular Collider hadron-hadron (FCC-hh) [17], respectively. The discovery of any Higgs boson beyond the SM will be unequivocal evidence for the existence of an extended Higgs sector. Therefore, probing Higgs sectors of extended models through direct searches for new Higgs bosons at high-energy colliders or through modifications to SM-like Higgs couplings tested by precision measurements of Higgs coupling take on a transcendental role [18]. The reason for this is that they open new routes to explore new physics effects.

Until now, direct and indirect searches for new physics at a weak scale have produced only unsuccessful results. However, new physics is expected to emerge at high masses, which means that it will be necessary to maximize the center-of-mass energy  $\sqrt{s}$  of current colliders so that new heavy particles can be produced in collisions. The mentioned above motivates the construction of more energetic colliders with higher luminosity  $\mathcal{L}$ . Therefore, the search for new physics beyond the SM remains a frontier in particle physics research.

The article is organized as follows. In Section II, we briefly review the BLHM. In Section III, we present and study the tree-level and one-loop decays of the Higgs boson  $H_0$ . In Section IV, we show the predictions of the BLHM in the production cross-sections of the  $H_0$  Higgs for the processes via gluon fusion. Finally, conclusions are presented in Section V.

## II. A BRIEF REVIEW OF THE BLHM

The BLHM [1–7] is based on two independent non-linear sigma models. With the first field  $\Sigma$ , the global symmetry  $SO(6)_A \times SO(6)_B$  is broken to the diagonal group  $SO(6)_V$  at the energy scale  $f$ , while with the second field  $\Delta$ , the global symmetry  $SU(2)_C \times SU(2)_D$  to the diagonal subgroup  $SU(2)$  to the scale  $F > f$ . In the first stage, 15 pseudo-Nambu-Goldstone bosons that are parameterized as

$$\Sigma = e^{i\Pi/f} e^{2i\Pi_h/f} e^{i\Pi/f}, \quad (1)$$

where  $\Pi$  and  $\Pi_h$  are complex and antisymmetric matrices given in Ref. [1]. Regarding the second stage of spontaneous symmetry-breaking, the pseudo-Nambu-Goldstone bosons of the field  $\Delta$  are parameterized as follows

$$\Delta = F e^{2i\Pi_d/F}, \quad \Pi_d = \chi_a \frac{\tau^a}{2} \quad (a = 1, 2, 3), \quad (2)$$

$\chi_a$  represents the Nambu-Goldstone fields and the  $\tau_a$  correspond to the Pauli matrices [1], which are the generators of the SU(2) group.

### A. The scalar sector

The BLHM Higgs fields,  $h_1$  and  $h_2$ , form the Higgs potential that undergoes spontaneous symmetry breaking [1, 3, 19]:

$$V_{Higgs} = \frac{1}{2}m_1^2 h_1^T h_1 + \frac{1}{2}m_2^2 h_2^T h_2 - B_\mu h_1^T h_2 + \frac{\lambda_0}{2}(h_1^T h_2)^2. \quad (3)$$

The symmetry-breaking mechanism is implemented in the BLHM when the Higgs doublets acquire their vacuum expectation values (VEVs),  $\langle h_1 \rangle^T = (v_1, 0, 0, 0)$  and  $\langle h_2 \rangle^T = (v_2, 0, 0, 0)$ . By demanding that these VEVs minimize the Higgs potential of Eq. (3), the following relations are obtained

$$v_1^2 = \frac{1}{\lambda_0} \frac{m_2}{m_1} (B_\mu - m_1 m_2), \quad (4)$$

$$v_2^2 = \frac{1}{\lambda_0} \frac{m_1}{m_2} (B_\mu - m_1 m_2). \quad (5)$$

These parameters can be expressed as follows

$$v^2 \equiv v_1^2 + v_2^2 = \frac{1}{\lambda_0} \left( \frac{m_1^2 + m_2^2}{m_1 m_2} \right) (B_\mu - m_1 m_2) \simeq (246 \text{ GeV})^2, \quad (6)$$

$$\tan \beta = \frac{v_1}{v_2} = \frac{m_2}{m_1}. \quad (7)$$

From the diagonalization of the mass matrix for the scalar sector, three non-physical fields  $G_0$  and  $G^\pm$ , two physical scalar fields  $H^\pm$  and three neutral physical scalar fields  $h_0$ ,  $H_0$  and  $A_0$  are generated [3, 20]. The lightest state,  $h_0$ , is identified as the scalar boson of the SM. The four parameters in the Higgs potential  $m_1$ ,  $m_2$ ,  $B_\mu$ , and  $\lambda_0$  can be replaced by another more phenomenologically accessible set. That is, the masses of the states  $h_0$  and  $A_0$ , the angle  $\beta$  and the VEV  $v$  [3]:

$$B_\mu = \frac{1}{2}(\lambda_0 v^2 + m_{A_0}^2) \sin 2\beta, \quad (8)$$

$$\lambda_0 = \frac{m_{h_0}^2}{v^2} \left( \frac{m_{h_0}^2 - m_{A_0}^2}{m_{h_0}^2 - m_{A_0}^2 \sin^2 2\beta} \right), \quad (9)$$

$$\tan \alpha = \frac{B_\mu \cot 2\beta + \sqrt{(B_\mu^2 / \sin^2 2\beta) - 2\lambda_0 B_\mu v^2 \sin 2\beta + \lambda_0^2 v^4 \sin^2 2\beta}}{B_\mu - \lambda_0 v^2 \sin 2\beta}, \quad (10)$$

$$m_{H_0}^2 = \frac{B_\mu}{\sin 2\beta} + \sqrt{\frac{B_\mu^2}{\sin^2 2\beta} - 2\lambda_0 B_\mu v^2 \sin 2\beta + \lambda_0^2 v^4 \sin^2 2\beta}, \quad (11)$$

$$m_\sigma^2 = (\lambda_{56} + \lambda_{65})f^2 = 2\lambda_0 f^2 K_\sigma, \quad (12)$$

$$1 < \tan \beta < \sqrt{\frac{2 + 2\sqrt{(1 - \frac{m_{h_0}^2}{m_{A_0}^2})(1 - \frac{m_{h_0}^2}{4\pi v^2})}}{\frac{m_{h_0}^2}{m_{A_0}^2}(1 + \frac{m_{A_0}^2 - m_{h_0}^2}{4\pi v^2})}} - 1. \quad (13)$$

The variables  $\lambda_{56}$  and  $\lambda_{65}$  in Eq. (12) represent the coefficients of the quartic potential defined in [1], both variables take values different from zero to achieve the collective breaking of the symmetry and generate a quartic coupling of the Higgs boson [1, 3].

## B. The gauge sector

The kinetic terms of the gauge fields in the BLHM are given as follows:

$$\mathcal{L} = \frac{f^2}{8} \text{Tr}(D_\mu \Sigma^\dagger D^\mu \Sigma) + \frac{F^2}{4} \text{Tr}(D_\mu \Delta^\dagger D^\mu \Delta), \quad (14)$$

where the covariant derivatives are given by

$$D_\mu \Sigma = \partial_\mu \Sigma + ig_A A_{1\mu}^a T_L^a \Sigma - ig_B \Sigma A_{2\mu}^a T_L^a + ig_Y B_\mu^3 (T_R^3 \Sigma - \Sigma T_R^3), \quad (15)$$

$$D_\mu \Delta = \partial_\mu \Delta + ig_A A_{1\mu}^a \frac{\tau^a}{2} \Delta - ig_B \Delta A_{2\mu}^a \frac{\tau^a}{2}. \quad (16)$$

$T_L^a$  are the generators of the group  $SO(6)_A$  corresponding to the subgroup  $SU(2)_{LA}$ , while  $T_R^3$  represents the third component of the  $SO(6)_B$  generators corresponding to the  $SU(2)_{LB}$  subgroup, these matrices are provided in [1].  $g_A$  and  $A_{1\mu}^a$  denote the gauge coupling and field associated with the gauge bosons of  $SU(2)_{LA}$ .  $g_B$  and  $A_{2\mu}^a$  represent the gauge coupling and the field associated with  $SU(2)_{LB}$ , while  $g_Y$  and  $B_\mu^3$  denote the hypercharge and the field.

When  $\Sigma$  and  $\Delta$  get their VEVs, the gauge fields  $A_{1\mu}^a$  and  $A_{2\mu}^a$  are mixed to form a massless triplet  $A_{0\mu}^a$  and a massive triplet  $A_{H\mu}^a$ ,

$$A_{0\mu}^a = \cos \theta_g A_{1\mu}^a + \sin \theta_g A_{2\mu}^a, \quad A_{H\mu}^a = \sin \theta_g A_{1\mu}^a - \cos \theta_g A_{2\mu}^a, \quad (17)$$

with the mixing angle

$$s_g \equiv \sin \theta_g = \frac{g_A}{\sqrt{g_A^2 + g_B^2}}, \quad c_g \equiv \cos \theta_g = \frac{g_B}{\sqrt{g_A^2 + g_B^2}}, \quad (18)$$

which are related to the electroweak gauge coupling  $g$  through

$$\frac{1}{g^2} = \frac{1}{g_A^2} + \frac{1}{g_B^2}. \quad (19)$$

On the other hand, the weak mixing angle is defined as

$$s_W \equiv \sin \theta_W = \frac{g_Y}{\sqrt{g^2 + g_Y^2}}, \quad (20)$$

$$c_W \equiv \cos \theta_W = \frac{g}{\sqrt{g^2 + g_Y^2}}. \quad (21)$$

### C. The Yang-Mills sector

The gauge boson self-interactions arise from the following Lagrangian terms:

$$\mathcal{L} = F_{1\mu\nu} F_1^{\mu\nu} + F_{2\mu\nu} F_2^{\mu\nu}, \quad (22)$$

where  $F_{1,2}^{\mu\nu}$  are given by

$$F_1^{\mu\nu} = \partial^\mu A_1^{\alpha\nu} - \partial^\nu A_1^{\alpha\mu} + g_A \sum_b \sum_c \epsilon^{abc} A_1^{b\mu} A_1^{c\nu}, \quad (23)$$

$$F_2^{\mu\nu} = \partial^\mu A_2^{\alpha\nu} - \partial^\nu A_2^{\alpha\mu} + g_B \sum_b \sum_c \epsilon^{abc} A_2^{b\mu} A_2^{c\nu}. \quad (24)$$

In these equations, the indices  $a$ ,  $b$ , and  $c$  run over the three gauge fields [21];  $\epsilon^{abc}$  is the anti-symmetric tensor.

### D. The fermion sector

To construct the Yukawa interactions in the BLHM, the fermions must be transformed under the group  $SO(6)_A$  or  $SO(6)_B$ . In this model, the fermion sector is divided into two parts. First, the sector of massive fermions is represented by Eq. (25). This sector includes the top and bottom quarks of the SM and a series of new heavy quarks arranged in four multiplets,  $Q$  and  $Q'$ , which transform under  $SO(6)_A$ , while  $U^c$  and  $U_5'^c$  are transformed under the group  $SO(6)_B$ . Second, the sector of light fermions contained in Eq. (26), in this expression, all the interactions of the remaining fermions of the SM with the exotic particles of the BLHM are generated.

For massive fermions, the Lagrangian that describes them is given by [1]

$$\mathcal{L}_t = y_1 f Q^T S \Sigma S U^c + y_2 f Q'^T \Sigma U^c + y_3 f Q'^T \Sigma U_5'^c + y_b f q_3^T (-2iT_R^2 \Sigma) U_b^c + h.c., \quad (25)$$

where  $S = \text{diag}(1, 1, 1, 1, -1, -1)$ . The explicit representation of the multiplets involved in Eq. (25) is provided in Refs. [1, 20]. For simplicity, the Yukawa couplings are assumed to be real  $y_1, y_2, y_3 \in R$ .

For light fermions, the corresponding Lagrangian is [1, 20, 21]

$$\mathcal{L}_{light} = \sum_{i=1,2} y_u f q_i^T \Sigma u_i^c + \sum_{i=1,2} y_d f q_i^T (-2iT_R^2 \Sigma) d_i^c + \sum_{i=1,2,3} y_e f l_i^T (-2iT_R^2 \Sigma) e_i^c + h.c. \quad (26)$$

### E. The currents sector

The Lagrangian that describes the interactions of fermions with the gauge bosons is [1, 20]

$$\begin{aligned} \mathcal{L} = & \bar{Q} \bar{\tau}^\mu D_\mu Q + \bar{Q}' \bar{\tau}^\mu D_\mu Q' - U^{c\dagger} \tau^\mu D_\mu U^c - U'^{c\dagger} \tau^\mu D_\mu U'^c - U_b^{c\dagger} \tau^\mu D_\mu U_b^c + \sum_{i=1,2} q_i^\dagger \tau^\mu D_\mu q_i \\ & + \sum_{i=1,2,3} l_i^\dagger \tau^\mu D_\mu l_i - \sum_{i=1,2,3} e_i^{c\dagger} \tau^\mu D_\mu e_i^c - \sum_{i=1,2} u_i^{c\dagger} \tau^\mu D_\mu u_i^c - \sum_{i=1,2} d_i^{c\dagger} \tau^\mu D_\mu d_i^c, \end{aligned} \quad (27)$$

where  $\tau^\mu$  and  $\bar{\tau}^\mu$  are defined according to [22]. On the other hand, the respective covariant derivatives are provided in Refs. [6, 7].

## III. HEAVY HIGGS BOSON DECAYS AT THE BLHM

Recently, the first experimental evidence for the decay of the Higgs boson of the SM ( $h_0^{SM}$ ) into a photon and a  $Z$  boson was presented, with a statistical significance of 3.4

standard deviations [23, 24]. The result is derived from a combined analysis of the searches performed by the ATLAS and CMS collaborations. In addition to this search channel, the diphoton decay of the SM Higgs is also a verified fact [25]. The  $h_0^{SM} \rightarrow \gamma\gamma, \gamma Z$  processes are essential particle physics as they are sensitive to possible contributions from physics beyond the SM and can even probe scenarios where the SM-like Higgs boson emerges. Although the  $h_0^{SM} \rightarrow \gamma\gamma, \gamma Z$  decay channels have small branching fractions, they provide a clean final state topology which can reconstruct the diphoton invariant mass and photon- $Z(\rightarrow ll, l = e \text{ or } \mu)$  invariant mass with high precision [23, 25]. A new window to explore physics not described by the SM has opened with the discovery of the first fundamental scalar particle  $h_0^{SM}$ . Many of the extended models postulate the existence of heavy states. Linked to this, the search for additional scalar particles is being carried out by the ATLAS and CMS collaborations at the CERN LHC using data from increasingly energetic collisions. These facts motivate our study of the production of the  $H_0$  Higgs of the BLHM at the LHC and the FCC-hh. For this purpose, we calculate the total decay width of the  $H_0$  Higgs, where we will consider direct search channels with SM final states. In the following, we describe the different decay modes of the Higgs boson  $H_0$ .

### A. Two-body decays of the Higgs boson $H_0$ at tree level

In the BLHM, the Feynman diagrams representing the two-body decays of the  $H_0$  Higgs at tree level are shown in Fig. 1. To calculate the partial decay widths of  $H_0$ , we use the Feynman rules for the interaction vertices provided in Refs. [5–7, 26, 27].

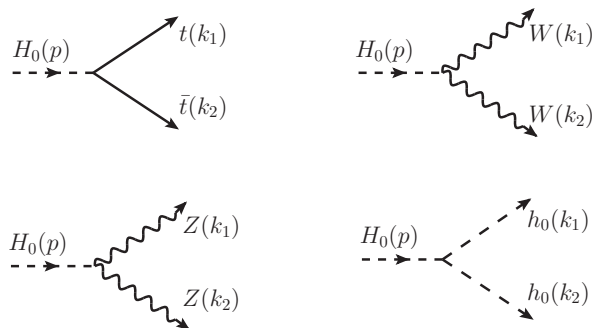


FIG. 1: Feynman diagrams corresponding to the two-body decays of the  $H_0$  Higgs at tree level.



The decay widths of  $H_0 \rightarrow \bar{t}t, WW, ZZ, h_0h_0$  can be written as follows

$$\Gamma(H_0 \rightarrow \bar{t}t) = \frac{N_c g_{H_0 tt}^2 m_{H_0}}{8\pi} \left(1 - \frac{4m_t^2}{m_{H_0}^2}\right)^{3/2}, \quad (28)$$

$$\Gamma(H_0 \rightarrow WW) = \frac{g_{H_0 WW}^2 m_{H_0}^3}{64\pi m_W^4} \sqrt{1 - \frac{4m_W^2}{m_{H_0}^2}} \left(1 - \frac{4m_W^2}{m_{H_0}^2} + \frac{12m_W^4}{m_{H_0}^4}\right), \quad (29)$$

$$\Gamma(H_0 \rightarrow ZZ) = \frac{g_{H_0 ZZ}^2 m_{H_0}^3}{128\pi m_Z^4} \sqrt{1 - \frac{4m_Z^2}{m_{H_0}^2}} \left(1 - \frac{4m_Z^2}{m_{H_0}^2} + \frac{12m_Z^4}{m_{H_0}^4}\right), \quad (30)$$

$$\Gamma(H_0 \rightarrow h_0h_0) = \frac{g_{H_0 h_0 h_0}^2}{32\pi m_{H_0}} \sqrt{1 - \frac{4m_{h_0}^2}{m_{H_0}^2}}, \quad (31)$$

where  $N_c = 3$ , is the color factor and  $g_{H_0 tt}, g_{H_0 WW}, g_{H_0 ZZ}$  and  $g_{H_0 h_0 h_0}$  represent the couplings of the interaction vertices involved in the tree-level processes, which are given in Refs. [5–7, 26, 27].

## B. Three-body decays of the Higgs boson $H_0$ at tree level

Concerning the three-body decays of the  $H_0$  Higgs, the Feynman diagrams that arise for these processes are shown in Fig. 2. The scalar particles and gauge bosons of the SM and the BLHM mediate these processes. The Feynman rules for the interaction vertices are given in Refs. [5–7, 26]. We only provide the decay amplitudes because the expressions generated for the partial widths are quite lengthy. The analytical expressions for the decay widths of the  $H_0$  Higgs decaying to three bodies can be calculated using the generic formula described in Eq. (32) [28, 29],

$$\frac{d\Gamma(H_0 \rightarrow ABC)}{dx_a dx_b} = \frac{m_{H_0}}{256\pi^3} |\mathcal{M}(H_0 \rightarrow ABC)|^2. \quad (32)$$

It is worth mentioning that for some decay channels of the  $H_0$  Higgs, specific interaction vertices ( $Z'WW$ ,  $h_0WW'$ , and  $h_0ZZ'$ ) cancel out. This happens because in the BLHM

the gauge couplings  $g_A$  and  $g_B$ , associated to the gauge bosons  $SU(2)_{LA}$  and  $SU(2)_{LB}$ , can be parametrized in a more phenomenological fashion in terms of a mixing angle  $\theta_g$ ,  $\tan \theta_g = g_A/g_B$ . For simplicity, it is assumed that  $\tan \theta_g = 1$  [6, 20], which implies that the gauge couplings  $g_A$  and  $g_B$  are equal, i.e.,  $\sin \theta_g = \cos \theta_g$  ( $s_g = c_g$ ). This fact leads to no contribution from specific decay amplitudes. The only contributing amplitudes are given in Eqs. (33)-(35).

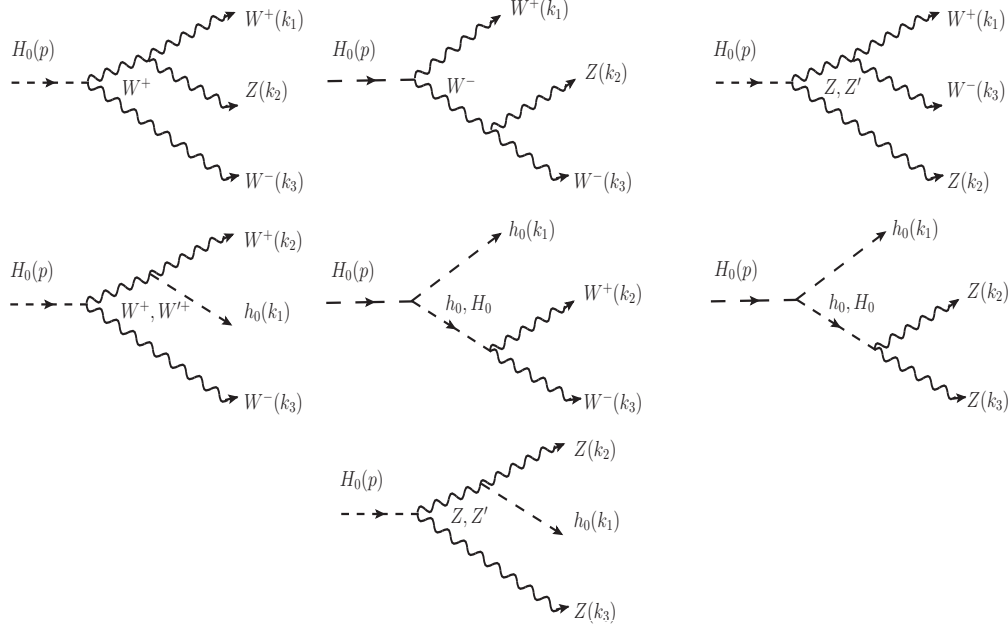


FIG. 2: Feynman diagrams corresponding to the three-body decays of the  $H_0$  Higgs at tree level.

$$\begin{aligned}
\mathcal{M}(H_0 \rightarrow W Z Z) = & \quad i g_{WWZ} \left[ - \frac{g_{H_0 WW}}{(k_1 + k_2)^2 - m_W^2} \left( (k_1^\mu + 2k_2^\mu) g^{\alpha\nu} - (2k_1^\nu + k_2^\nu) g^{\alpha\mu} \right. \right. \\
& + \left( -2k_2^\alpha + \frac{m_Z^2}{m_W^2} (k_1^\alpha + k_2^\alpha) \right) g^{\mu\nu} + \frac{(k_1^\alpha + k_2^\alpha)(k_1^\mu k_2^\nu - k_2^\mu k_1^\nu)}{m_W^2} \Big) \\
& + \frac{g_{H_0 WW}}{(k_2 + k_3)^2 - m_W^2} \left( (2k_2^\alpha + k_3^\alpha) g^{\mu\nu} + \frac{(k_3^\alpha k_2^\nu - k_2^\alpha k_3^\nu)(k_2^\mu + k_3^\mu)}{m_W^2} \right. \\
& + \left( -2k_2^\mu + \frac{m_Z^2}{m_W^2} (k_2^\mu + k_3^\mu) \right) g^{\alpha\nu} - (k_2^\nu + 2k_3^\nu) g^{\alpha\mu} \Big) \\
& + \frac{g_{H_0 ZZ}}{(k_1 + k_3)^2 - m_Z^2} \left( - (k_1^\mu + 2k_3^\mu) g^{\alpha\nu} - (k_1^\nu - k_3^\nu) g^{\alpha\mu} \right. \\
& \left. \left. + (2k_1^\alpha + k_3^\alpha) g^{\mu\nu} + \frac{(k_3^\alpha k_1^\mu - k_1^\alpha k_3^\mu)(k_1^\nu + k_3^\nu)}{m_Z^2} \right) \right] \epsilon_\mu^*(k_1) \epsilon_\nu^*(k_2) \epsilon_\alpha^*(k_3), \quad (33)
\end{aligned}$$

$$\mathcal{M}(H_0 \rightarrow h_0 WW) = i \left[ \left( \frac{g_{h_0 H_0 H_0} g_{H_0 WW}}{(k_2+k_3)^2 - m_{H_0}^2} + \frac{g_{H_0 h_0 h_0} g_{h_0 WW}}{(k_2+k_3)^2 - m_{h_0}^2} + \frac{g_{H_0 WW} g_{h_0 WW}}{(k_1+k_2)^2 - m_W^2} \right) g^{\mu\nu} \right. \\ \left. - \frac{g_{h_0 WW} g_{H_0 WW} (k_1^\mu + k_2^\mu)(k_1^\nu + k_2^\nu)}{m_W^2 ((k_1+k_2)^2 - m_W^2)} \right] \epsilon_\mu^*(k_2) \epsilon_\nu^*(k_3), \quad (34)$$

$$\mathcal{M}(H_0 \rightarrow h_0 ZZ) = i \left[ \left( \frac{g_{h_0 H_0 H_0} g_{H_0 ZZ}}{(k_2+k_3)^2 - m_{H_0}^2} + \frac{g_{H_0 h_0 h_0} g_{h_0 ZZ}}{(k_2+k_3)^2 - m_{h_0}^2} + \frac{g_{H_0 ZZ} g_{h_0 ZZ}}{(k_1+k_2)^2 - m_Z^2} \right) g^{\mu\nu} \right. \\ \left. - \frac{g_{h_0 ZZ} g_{H_0 ZZ} (k_1^\mu + k_2^\mu)(k_1^\nu + k_2^\nu)}{m_Z^2 ((k_1+k_2)^2 - m_Z^2)} \right] \epsilon_\mu^*(k_2) \epsilon_\nu^*(k_3). \quad (35)$$

### C. Two-body decays of the Higgs boson $H_0$ at one-loop level

This subsection determines the amplitudes and partial decay widths of the  $H_0$  Higgs at the one-loop level. In Fig. 3, we show the Feynman diagrams associated with the  $H_0 \rightarrow \gamma\gamma, \gamma Z, gg$  decays which are mediated by fermions ( $t; T; T^{2/3}; T_5; T_6$ ) and gauge bosons ( $W^\pm; W'^\pm$ ) of the SM and BLHM. These  $H_0$  decays are absent at the tree level in the BLHM. However, they arise at a one-loop level, which is of great interest since they not only help to examine higher-order corrections to the theory but also provide information about possible contributions from new particles circulating in the loop.

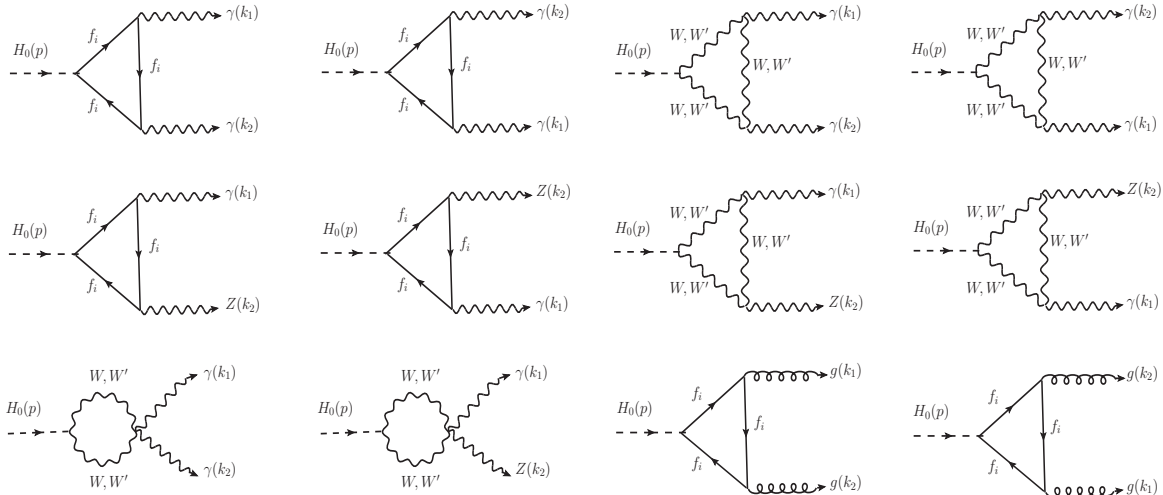


FIG. 3: Feynman diagrams corresponding to the two-body decays of the  $H_0$  Higgs at one-loop level. The notation  $f_i$  represents the  $t, T, T^{2/3}, T_5, T_6$  quarks.

In the following, all calculations at the one-loop level will be carried out using the unitary gauge and the Passarino-Veltman (PV) reduction scheme [30]. In this way, we find that the total amplitude for the first decay  $H_0 \rightarrow \gamma\gamma$  can be written as

$$\mathcal{M}(H_0 \rightarrow \gamma\gamma) = (A_f^{\gamma\gamma} + A_W^{\gamma\gamma} + A_{W'}^{\gamma\gamma})(k_1^\nu k_2^\mu - k_1 \cdot k_2 g^{\mu\nu})\epsilon_\mu^*(k_1)\epsilon_\nu^*(k_2), \quad (36)$$

where the form factors  $A_f^{\gamma\gamma}$ ,  $A_W^{\gamma\gamma}$ ,  $A_{W'}^{\gamma\gamma}$  are defined as follows

$$A_f^{\gamma\gamma} = \frac{N_c}{2\pi^2 m_{H_0}^2} \sum_{f=t,T,T_5,T_6,T^{2/3}} g_{H_0 f f} (g_{A f f})^2 m_f Q_f \left( 2 - (m_{H_0}^2 - 4m_f^2) C_0(m_{H_0}^2, 0, 0, m_f^2, m_f^2, m_f^2) \right), \quad (37)$$

$$A_W^{\gamma\gamma} = \frac{g_{H_0 W W} (g_{W W A})^2}{8\pi^2 m_{H_0}^2} \left( 6(m_{H_0}^2 - 2m_W^2) C_0(m_{H_0}^2, 0, 0, m_W^2, m_W^2, m_W^2) - \frac{m_{H_0}^2}{m_W^2} - 6 \right), \quad (38)$$

$$A_{W'}^{\gamma\gamma} = \frac{g_{H_0 W' W'} (g_{W' W' A})^2}{8\pi^2 m_{H_0}^2} \left( 6(m_{H_0}^2 - 2m_{W'}^2) C_0(m_{H_0}^2, 0, 0, m_{W'}^2, m_{W'}^2, m_{W'}^2) - \frac{m_{H_0}^2}{m_{W'}^2} - 6 \right). \quad (39)$$

The labels  $f$  and  $W$  ( $W'$ ) of the form factors  $A_f^{\gamma\gamma}$  and  $A_W^{\gamma\gamma}$  ( $A_{W'}^{\gamma\gamma}$ ), respectively, represent the contributions generated due to the quarks and gauge bosons circulating in the loop of the diphoton decay of  $H_0$  Higgs. On the other hand,  $C_0(m_{H_0}^2, 0, 0, m_f^2, m_f^2, m_f^2)$ ,  $C_0(m_{H_0}^2, 0, 0, m_W^2, m_W^2, m_W^2)$  and  $C_0(m_{H_0}^2, 0, 0, m_{W'}^2, m_{W'}^2, m_{W'}^2)$  denote the scalar functions of PV.

Using Eq. (36), we find that the decay width for the  $H_0 \rightarrow \gamma\gamma$  process is

$$\Gamma(H_0 \rightarrow \gamma\gamma) = \frac{1}{64\pi} |A_f^{\gamma\gamma} + A_W^{\gamma\gamma} + A_{W'}^{\gamma\gamma}|^2 m_{H_0}^3. \quad (40)$$

The one-loop decay amplitude for the second process  $H_0 \rightarrow \gamma Z$  is

$$\mathcal{M}(H_0 \rightarrow \gamma Z) = (A_f^{\gamma Z} + A_W^{\gamma Z} + A_{W'}^{\gamma Z})(k_1^\nu k_2^\mu - k_1 \cdot k_2 g^{\mu\nu})\epsilon_\mu^*(k_1)\epsilon_\nu^*(k_2), \quad (41)$$

with

$$A_f^{\gamma Z} = \frac{N_c}{2\pi^2(m_{H_0}^2 - m_Z^2)^2} \sum_{f=t,T,T_5,T_6,T^{2/3}} m_f Q_f \left[ g_{H_0 f f} g_{A f f} g_{Z f f} \left( (m_{H_0}^2 - m_Z^2)(m_Z^2 + 4m_f^2 - m_{H_0}^2) \right. \right. \\ \left. \left. \times C_0(m_{H_0}^2, 0, 0, m_f^2, m_f^2, m_f^2) + 2 \right) - 2m_Z^2 \left( B_0(m_Z^2, m_f^2, m_f^2) - B_0(m_{H_0}^2, m_f^2, m_f^2) \right) \right], \quad (42)$$

$$A_W^{\gamma Z} = \frac{g_{H_0 W W} g_{W W A} g_{W W Z}}{16\pi^2 t_W^4 (1-t_Z^2) m_{H_0}^2} \left[ \left( 12t_W^4 - 2t_W^2(t_Z^2 - 1) - t_Z^2 \right) \right. \\ \times \left( t_Z^2 (B_0(m_{H_0}^2, m_W^2, m_W^2) - B_0(m_Z^2, m_W^2, m_W^2) - 1) + 1 \right) \\ \left. - 2t_W^2(t_Z^2 - 1) \left( 12t_W^4 + 6t_W^2(t_Z^2 - 1) - t_Z^2(2t_Z^2 - 1) \right) \right. \\ \left. \times m_{H_0}^2 C_0(m_{H_0}^2, m_Z^2, 0, m_W^2, m_W^2, m_W^2) \right], \quad (43)$$

and

$$A_{W'}^{\gamma Z} = \frac{g_{H_0 W' W'} g_{W' W' A} g_{W' W' Z}}{16\pi^2 t_{W'}^4 (1-t_Z^2) m_{H_0}^2} \left[ \left( 12t_{W'}^4 - 2t_{W'}^2(t_Z^2 - 1) - t_Z^2 \right) \right. \\ \times \left( t_Z^2 (B_0(m_{H_0}^2, m_{W'}^2, m_{W'}^2) - B_0(m_Z^2, m_{W'}^2, m_{W'}^2) - 1) + 1 \right) \\ \left. - 2t_{W'}^2(t_Z^2 - 1) \left( 12t_{W'}^4 + 6t_{W'}^2(t_Z^2 - 1) - t_Z^2(2t_Z^2 - 1) \right) \right. \\ \left. \times m_{H_0}^2 C_0(m_{H_0}^2, m_Z^2, 0, m_{W'}^2, m_{W'}^2, m_{W'}^2) \right], \quad (44)$$

being  $t_W = \frac{m_W}{m_{H_0}}$ ,  $t_Z = \frac{m_Z}{m_{H_0}}$  and  $t_{W'} = \frac{m_{W'}}{m_{H_0}}$ . It is worth mentioning that the form factors  $A_f^{\gamma Z}$ ,  $A_W^{\gamma Z}$  and  $A_{W'}^{\gamma Z}$  provide finite results, i.e. these are free of ultraviolet divergences. For the  $H_0 \rightarrow \gamma Z$  decay, their corresponding decay width is

$$\Gamma(H_0 \rightarrow \gamma Z) = \frac{1}{32\pi m_{H_0}^3} |A_f^{\gamma Z} + A_W^{\gamma Z} + A_{W'}^{\gamma Z}|^2 (m_{H_0}^2 - m_Z^2)^3. \quad (45)$$

Finally, the decay amplitude of the process  $H_0 \rightarrow gg$  is as follows

$$\mathcal{M}(H_0 \rightarrow gg) = A^{gg}(k_1^\nu k_2^\mu - k_1 \cdot k_2 g^{\mu\nu}) \epsilon_\mu^{*a}(k_1) \epsilon_\nu^{*b}(k_2) \delta_{ab}, \quad (46)$$

where

$$A^{gg} = \frac{N_c}{4\pi^2 m_{H_0}^2} \sum_{f=t,T,T_5,T_6,T^{2/3}} g_{H_0 f f} (g_{g s f f})^2 m_f \left( 2 - (m_{H_0}^2 - 4m_f^2) C_0(m_{H_0}^2, 0, 0, m_f^2, m_f^2, m_f^2) \right). \quad (47)$$

The corresponding decay width for the  $H_0 \rightarrow gg$  process is given by:

$$\Gamma(H_0 \rightarrow gg) = \frac{1}{8\pi} |A^{gg}|^2 m_{H_0}^3. \quad (48)$$

#### IV. NUMERICAL RESULTS

To carry out our numerical analysis of the  $H_0$  Higgs production in the context of the BLHM, we briefly review some free parameters of the model of interest and provide in Table I the values assigned to the remaining free parameters.

As discussed in Refs. [5, 7], the three Yukawa couplings,  $y_1$ ,  $y_2$ , and  $y_3$  generate two study scenarios in the BLHM:

- Scenario **a** ( $y_2 < y_3$ ),  $y_1 = 0.61$ ,  $y_2 = 0.35$  and  $y_3 = 0.84$  [5–7],
- Scenario **b** ( $y_2 > y_3$ ),  $y_1 = 0.61$ ,  $y_2 = 0.84$  and  $y_3 = 0.35$  [5–7].

The restrictions on the Yukawa couplings arise due to perturbativity requirements that set an upper bound of  $4\pi$  on  $y_i$ ,  $i = 1, 2, 3$  [31]. On the other hand, the BLHM is designed to overcome the fine-tuning problem, which suggests that the masses of the new quarks must be less than about 2 TeV [1]. The expressions for the masses of the new heavy quarks involved in our calculations are, in turn, directly related to the Yukawa couplings  $y_i$ . In this way, scenarios **a** and **b** mentioned above offer realistic values of the Yukawa couplings that evade the fine-tuning constraints and satisfy the perturbativity requirements. In the following numerical analysis, our results are generated only for scenario *a*. Scenario *b* provides nearly identical results. The other input parameters involved in our analysis of the production of the  $H_0$  Higgs are shown in Table I.

TABLE I: Values assigned to the free parameters involved in our numerical analysis at the BLHM.

| Parameter    | Value            | Reference   |
|--------------|------------------|-------------|
| $m_{h_0}$    | 125.25 GeV       | [32]        |
| $m_{H_0}$    | 1015 GeV         | [33]        |
| $\tan \beta$ | 3                | [5–7]       |
| $g_A = g_B$  | $\sqrt{2}g$      | [5–7]       |
| $f$          | [1000, 3000] GeV | [1, 3, 5–7] |
| $F$          | [3000, 6000] GeV | [1, 3, 5–7] |

Due to the characteristics of the BLHM, this is based on two independent global symmetries that break into diagonal subgroups at different energy scales,  $f$  and  $F$ . These scales represent the scales of the new physics. Therefore, it is convenient to analyze the  $H_0$  production cross-section as a function of the energy scales  $f$  and  $F$  since the masses of the particles circulating in the loop of the  $H_0 \rightarrow \gamma\gamma, \gamma Z, gg$  processes depend on the scales  $f$  and  $F$ . On the other hand, one-loop decays of  $H_0$  into  $\gamma\gamma$ ,  $\gamma Z$ , and  $gg$  will be helpful to test the consistency of the current parameter space of the BLHM.

For the purposes mentioned above, we begin by presenting a numerical analysis of the decay widths for the  $H_0 \rightarrow tt, h_0 h_0, gg, WW, ZZ, h_0 WW, h_0 ZZ, WWZ, \gamma\gamma, \gamma Z$  processes. In this way, in Fig. 4 we show the behavior of  $\Gamma(H_0 \rightarrow X)$  vs.  $f$  and  $\Gamma(H_0 \rightarrow X)$  vs.  $F$ , where  $\Gamma(H_0 \rightarrow X)$  denotes the partial decay width of the  $H_0$  Higgs. From the first plot (see Fig. 4(a)), we can appreciate that the dominant and subdominant contributions to the decay width of  $H_0$  ( $\Gamma_{H_0}$ ) over the whole analysis interval of scale  $f$  come from the tree-level decays of  $H_0$  into  $t\bar{t}$  and  $h_0 h_0$ , respectively. The numerical contributions of these decays are  $\Gamma(H_0 \rightarrow t\bar{t}) \sim 10^0$  GeV and  $\Gamma(H_0 \rightarrow h_0 h_0) \sim 10^{-1}$  GeV. For this last contribution, the decay channels  $H_0 \rightarrow gg$  and  $H_0 \rightarrow WW$  also contribute with the same order of magnitude although slightly smaller than  $\Gamma(H_0 \rightarrow h_0 h_0)$ . Notice that the  $H_0 \rightarrow gg$  process is a one-loop decay. Other decay modes that contribute in lower order but contribute significantly to  $\Gamma_{H_0}$  are the  $H_0 \rightarrow ZZ, h_0 WW, h_0 ZZ, WWZ$  decays, whose associated decay widths are of  $10^{-2} - 10^{-3}$  GeV when  $f \in [1000, 3000]$  GeV, which are all tree-level decays. For the remaining one-loop decays, we find that the  $H_0 \rightarrow \gamma\gamma, \gamma Z$  decays provide suppressed

contributions to the decay width of the  $H_0$  Higgs:  $\Gamma(H_0 \rightarrow \gamma\gamma) \sim \Gamma(H_0 \rightarrow \gamma Z) \sim 10^{-4}$  GeV. Regarding the second plot (see Fig. 4(b)) which examines the dependence of  $\Gamma(H_0 \rightarrow X)$  on the energy scale  $F$ , we observe that the largest contributions to  $\Gamma_{H_0}$  are again generated by the  $H_0 \rightarrow \bar{t}t, h_0h_0$  decays:  $\Gamma(H_0 \rightarrow \bar{t}t) \sim 10^0$  GeV and  $\Gamma(H_0 \rightarrow h_0h_0) \sim 10^{-1}$  GeV for the interval of  $F = [3000, 6000]$  GeV. The processes  $H_0 \rightarrow gg, WW$  and  $H_0 \rightarrow ZZ, h_0WW, h_0ZZ$  also contribute considerably to the decay width of  $H_0$ , for these decays we find that the corresponding numerical estimates are  $\Gamma(H_0 \rightarrow gg) \sim \Gamma(H_0 \rightarrow WW) \sim 10^{-1}$  GeV and  $\Gamma(H_0 \rightarrow ZZ) \sim \Gamma(H_0 \rightarrow h_0WW) \sim \Gamma(H_0 \rightarrow h_0ZZ) \sim 10^{-2}$  GeV. Finally, the curves that provide the most suppressed contributions compared to the main contribution come from the  $H_0 \rightarrow WWZ$  and  $H_0 \rightarrow \gamma\gamma, \gamma Z$  decays, their predicted numerical magnitudes are 3 and 4 orders of magnitude smaller than  $\Gamma(H_0 \rightarrow \bar{t}t)$ , while the  $F$  scale acquires values in the range of 3000 to 6000 GeV. In summary, the numerical evaluation tells us that the tree-level decay channel  $H_0 \rightarrow \bar{t}t$  provides the most significant contribution to the  $H_0$  decay width. In contrast, the  $H_0 \rightarrow \gamma Z$  decay at the one-loop level generates the most minor contribution. On the other hand, we find that  $\Gamma(H_0 \rightarrow X)$  shows a greater sensitivity to the  $f$  scale compared to another scale of the new physics,  $F$ .

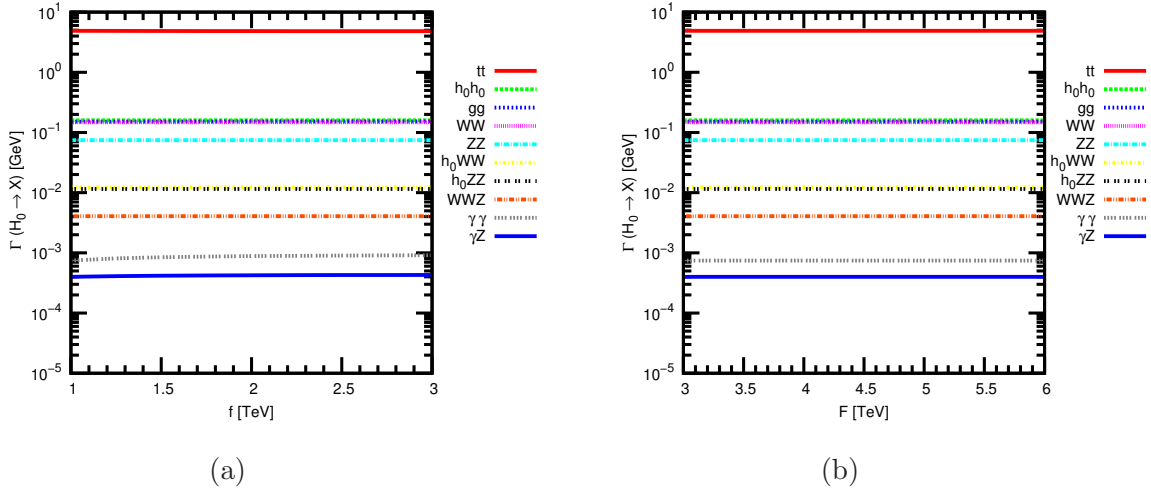


FIG. 4: Decay widths for the  $H_0 \rightarrow X$  processes where  $X = tt, h_0h_0, gg, WW, ZZ, h_0WW, h_0ZZ, WWZ, \gamma\gamma, \gamma Z$ . a)  $\Gamma(H_0 \rightarrow X)$  as a function of the  $f$  energy scale (with the fixed value of  $F = 4000$  GeV). b)  $\Gamma(H_0 \rightarrow X)$  as a function of the  $F$  energy scale (with the fixed value of  $f = 1000$  GeV).

We also calculate the branching ratios of the Higgs boson  $H_0$  as a function of



the energy scale  $f$  and  $F$ , as shown in Fig. 5. The plots are obtained considering the total decay width of the  $H_0$  Higgs, which contains the following decay modes:  $\bar{t}t, WW, ZZ, h_0h_0, h_0WW, h_0ZZ, WWZ, \gamma\gamma, \gamma Z, gg$ . From Fig. 5(a), we can see the curves that represent the estimates of the branching ratios versus the  $f$  scale when it takes values from 1000 to 3000 GeV. The  $H_0 \rightarrow \bar{t}t$  decay yields the highest contribution; its associated branching ratio is  $\text{Br}(H_0 \rightarrow \bar{t}t) \sim 10^{-1}$ . On the opposite side, we find that the most suppressed contribution is generated by the  $H_0 \rightarrow \gamma Z$  decay whose numerical magnitude of its branching ratio is  $10^{-5}$ . The remaining branching ratios turn out to be  $\text{Br}(H_0 \rightarrow h_0h_0) \sim \text{Br}(H_0 \rightarrow gg) \sim \text{Br}(H_0 \rightarrow WW) \sim \text{Br}(H_0 \rightarrow ZZ) \sim 10^{-2}$ ,  $\text{Br}(H_0 \rightarrow h_0WW) \sim \text{Br}(H_0 \rightarrow h_0ZZ) \sim 10^{-3}$  and  $\text{Br}(H_0 \rightarrow WWZ) \sim \text{Br}(H_0 \rightarrow \gamma\gamma) \sim 10^{-4}$  for  $f = [1000, 3000]$  GeV. Concerning Fig. 5(b), in this figure, we describe the behavior of  $\text{Br}(H_0 \rightarrow X)$  when the energy scale  $F$  takes values within the set analysis interval. As can be appreciated in the corresponding plot, the dominant branching ratios correspond to the tree-level decays ( $H_0 \rightarrow \bar{t}t, h_0h_0$ ) of the  $H_0$  Higgs while the minor contributions arise for one-loop decays ( $H_0 \rightarrow \gamma\gamma, \gamma Z$ ):  $\text{Br}(H_0 \rightarrow \bar{t}t) = 8.97 \times 10^{-1}$ ,  $\text{Br}(H_0 \rightarrow h_0h_0) = 2.92 \times 10^{-2}$ ,  $\text{Br}(H_0 \rightarrow \gamma\gamma) = 1.36 \times 10^{-4}$  and  $\text{Br}(H_0 \rightarrow \gamma Z) = 7.33 \times 10^{-5}$ . For these cases, the numerical predictions of  $\text{Br}(H_0 \rightarrow X)$  produce constant values over the whole range of  $F$  analysis, this also happens for the rest of the  $H_0$  decays, specifically  $H_0 \rightarrow gg, WW, ZZ, h_0WW, h_0ZZ, WWZ$  which generate the following branching ratios:  $\text{Br}(H_0 \rightarrow gg) = 2.78 \times 10^{-2}$ ,  $\text{Br}(H_0 \rightarrow WW) = 2.71 \times 10^{-2}$ ,  $\text{Br}(H_0 \rightarrow ZZ) = 1.37 \times 10^{-2}$ ,  $\text{Br}(H_0 \rightarrow h_0WW) = 2.25 \times 10^{-3}$ ,  $\text{Br}(H_0 \rightarrow h_0ZZ) = 2.12 \times 10^{-3}$  and  $\text{Br}(H_0 \rightarrow WWZ) = 7.45 \times 10^{-4}$ . From Figs. 5(a) and 5(b), we find that as  $f$  takes values closer to 3000 GeV, the magnitudes of the branching ratios are slightly larger. Thereby,  $\text{Br}(H_0 \rightarrow X)$  is sensitive to variations in the energy scale  $f$ . The above effect does not happen when we vary  $\text{Br}(H_0 \rightarrow X)$  versus the  $F$  scale; this is because, in the study scenario of our choice, the condition  $c_g = s_g$  removes from the interaction vertices (in most of them) the dependence on the  $F$  scale.

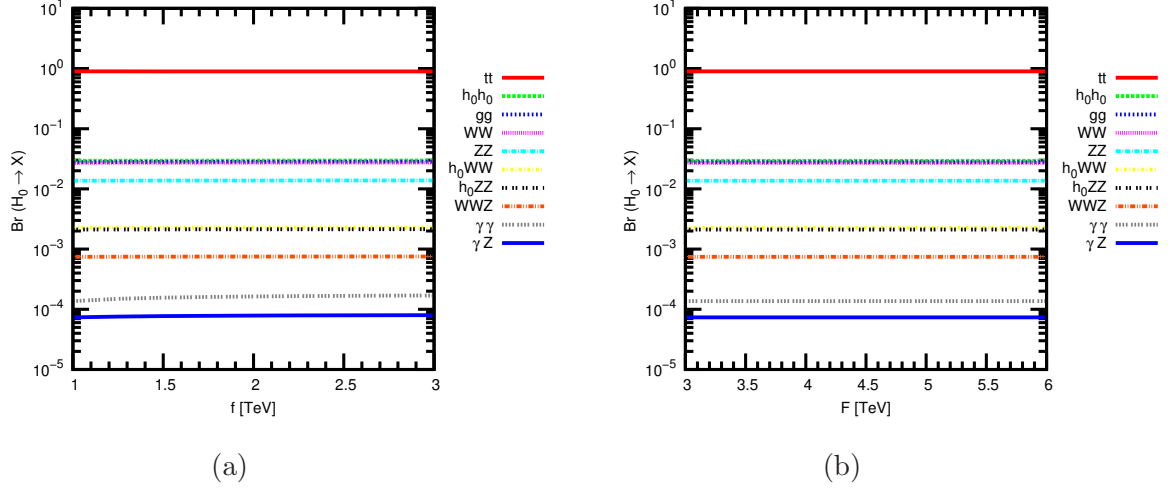


FIG. 5: The branching ratios for the  $H_0 \rightarrow X$  processes where  $X = tt, h_0h_0, gg, WW, ZZ, h_0WW, h_0ZZ, WWZ, \gamma\gamma, \gamma Z$ . a)  $\text{Br}(H_0 \rightarrow X)$  as a function of the  $f$  energy scale (with the fixed value of  $F = 4000$  GeV). b)  $\text{Br}(H_0 \rightarrow X)$  as a function of the  $F$  energy scale (with the fixed value of  $f = 1000$  GeV).

#### A. Higgs boson production $H_0$ of the BLHM at the LHC and the FCC-hh

We present an approximate study of the production cross-section of the  $H_0$  Higgs in the BLHM, which have decay channels  $\gamma\gamma, \gamma Z$ , and  $gg$ . For this purpose, we employ the Breit-Wigner resonant cross-section [28]. In this approximation, the production cross-section via gluon fusion can be calculated as follows,

$$\sigma(gg \rightarrow H_0 \rightarrow Y) = \frac{\pi}{36} \frac{\text{Br}(H_0 \rightarrow gg) \text{Br}(H_0 \rightarrow Y)}{m_{H_0}^2}, \quad (49)$$

where  $Y = \gamma\gamma, \gamma Z, gg$ . The cross-section  $\sigma(gg \rightarrow H_0 \rightarrow Y)$  is determined just at the resonance of the  $H_0$  Higgs. Although the method of analysis proposed in this subsection approximates the production mechanism of a massive scalar particle via gluon fusion, it could provide experimental guidance for the search for new heavy particles of the TeV order.

Based on previous studies where the sensitivity of the  $H_0$  partial decay widths and branching ratios on the  $F$  energy scale has been analyzed, the numerical estimates suggest that both  $\Gamma(H_0 \rightarrow X)$  and  $\text{Br}(H_0 \rightarrow X)$  show almost negligible sensitivity to the  $F$  energy scale. Thereby, we compute the  $H_0$  production cross-section only as a function of

the parameter  $f$  as shown in Fig. 6. In this figure, we observe that the curve providing the largest contribution is generated by the production cross-section of  $H_0$  with  $gg$  final states,  $\sigma(gg \rightarrow H_0 \rightarrow gg) = [25.45, 26.48]$  fb when  $f = [1000, 3000]$  GeV. On the other hand, the weakest contributions arise for  $\sigma(gg \rightarrow H_0 \rightarrow \gamma\gamma) = [1.25, 1.59] \times 10^{-1}$  fb and  $\sigma(gg \rightarrow H_0 \rightarrow \gamma Z) = [6.72, 7.46] \times 10^{-2}$  fb. Additionally, we discuss the behavior of  $\sigma(gg \rightarrow H_0 \rightarrow Y)$  vs.  $m_{H_0}$  as can be seen in Fig. 7. For the energy scale  $f$ , we assign fixed values such as 1000 GeV and 2000 GeV. With these input values for  $f$ , we generate the curves shown in Figs. 7(a) and 7(b). Based on the corresponding figures and the numerical estimations, we obtain that the dominant contribution to  $\sigma(gg \rightarrow H_0 \rightarrow Y)$  is reached through the  $H_0 \rightarrow gg$  decay channel when  $f = 1000$  GeV, its production cross-section is  $\sigma(gg \rightarrow H_0 \rightarrow gg) = [26.73, 1.68 \times 10^{-1}]$  fb for  $m_{H_0} = [1000, 3000]$  GeV. The subdominant contribution emerges when  $f = 2000$  GeV being  $\sigma(gg \rightarrow H_0 \rightarrow gg) = [26.61, 3.08 \times 10^{-1}]$  fb. The other curves generate slightly more suppressed contributions than the main contribution;  $\sigma(gg \rightarrow H_0 \rightarrow \gamma\gamma) = [1.29 \times 10^{-1}, 2.21 \times 10^{-2}]$  fb and  $\sigma(gg \rightarrow H_0 \rightarrow \gamma Z) = [7.15 \times 10^{-2}, 7.14 \times 10^{-3}]$  fb while  $f = 1000$  GeV, and  $\sigma(gg \rightarrow H_0 \rightarrow \gamma\gamma) = [1.57 \times 10^{-1}, 3.04 \times 10^{-2}]$  fb and  $\sigma(gg \rightarrow H_0 \rightarrow \gamma Z) = [7.75 \times 10^{-2}, 1.02 \times 10^{-2}]$  fb when  $f = 2000$  GeV.

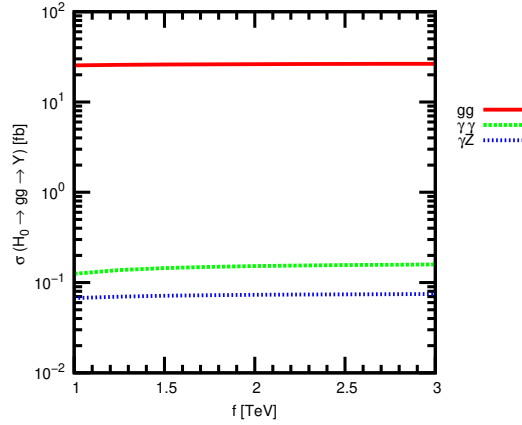


FIG. 6: The production cross-section of the  $H_0$  Higgs via gluon fusion as a function of the energy scale  $f$  (with the fixed value of  $F = 4000$  GeV).

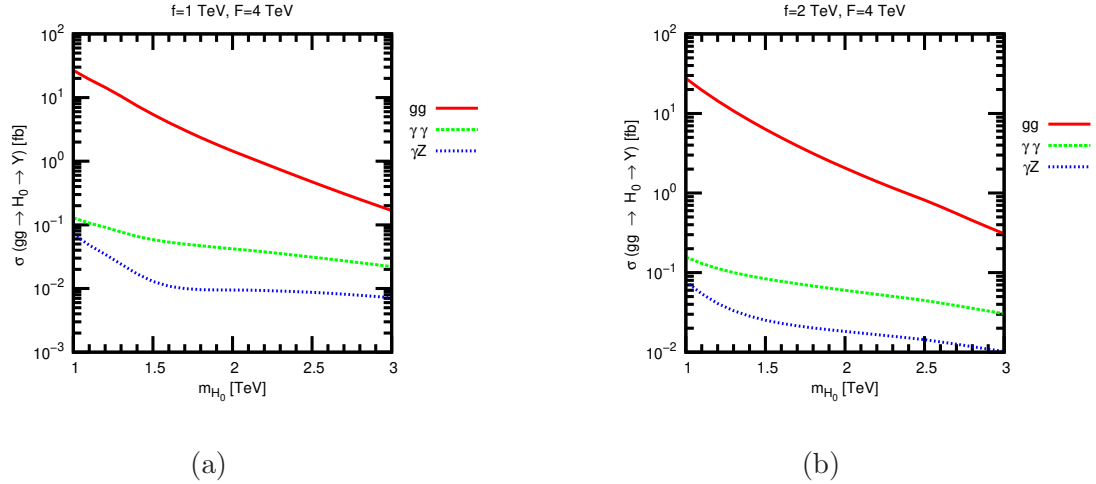


FIG. 7: The production cross-section of the  $H_0$  Higgs via gluon fusion as a function of  $m_{H_0}$  with a)  $f = 1$  TeV and b)  $f = 2$  TeV.

In the experimental scenario, the heavy Higgs production mechanism such as the  $H_0$  Higgs of the BLHM could be studied in the context of the LHC and its upgrades (High Luminosity (HL)-LHC, High Energy (HE)-LHC) or at future colliders like the FCC-hh. After LHC Long Shutdown 2, the expected integrated luminosity of the LHC in Run 3 is approximately  $450 \text{ fb}^{-1}$  [35]. On the other hand, the HL-LHC [17, 34, 36] is planned to operate at a center-of-mass energy of 14 TeV with an integrated luminosity of  $3\,000 \text{ fb}^{-1}$  while the HE-LHC [17, 34, 36] would provide  $pp$  collisions with a center-of-mass energy of 27 TeV and an integrated luminosity of  $10\,000 \text{ fb}^{-1}$ . In the future experiment, the FCC-hh [17, 36, 37] is designed to collect a total integrated luminosity of  $30\,000 \text{ fb}^{-1}$  operating at a center-of-mass energy of 100 TeV. Considering the production cross-sections  $\sigma(gg \rightarrow H_0 \rightarrow Y)$  and the expected integrated luminosities of the colliders mentioned above, we can obtain an estimate of the number of events that could be observed at the colliders for the processes of interest. For the purpose of generating a benchmark, considering  $m_{H_0} \approx 1000 \text{ GeV}$ , we provide in Tables II-IV the expected events related to  $H_0 \rightarrow gg, \gamma\gamma, \gamma Z$  decays when the scale of the new physics  $f$  takes specific values such as 1000, 2000, and 3000 GeV. According to the numerical data, the one-loop decay channel of the  $H_0$  Higgs corresponding to two gluons would be of great interest for the search of the hypothetical heavy particle, the  $H_0$  Higgs of the BLHM. Concerning the  $H_0 \rightarrow \gamma\gamma, \gamma Z$  decays, their respective expected event magnitudes also promise a very optimistic scenario as they appear to be within the

measurement range of the previously proposed future colliders.

TABLE II: The number of expected events related to  $H_0 \rightarrow gg$  decay.

| $f$ [TeV] | Number of expected events at the colliders: |  |   |   |
|-----------|---|--|---|---|
|           | LHC   | HL-LHC                                 | HE-LHC                                  | FCC-hh                                  |
|           | $\mathcal{L} = 450 \text{ fb}^{-1}$         | $\mathcal{L} = 3\,000 \text{ fb}^{-1}$ | $\mathcal{L} = 10\,000 \text{ fb}^{-1}$ | $\mathcal{L} = 30\,000 \text{ fb}^{-1}$ |
| 1         | 11 453                                      | 76 355                                 | 254 516                                 | 763 548                                 |
| 2         | 11 809                                      | 78 731                                 | 262 438                                 | 787 315                                 |
| 3         | 11 914                                      | 79 431                                 | 264 769                                 | 794 308                                 |

TABLE III: The number of expected events related to  $H_0 \rightarrow \gamma\gamma$  decay.

| $f$ [TeV] | Number of expected events at the colliders: |  |   |   |
|-----------|---|--|---|---|
|           | LHC   | HL-LHC                                 | HE-LHC                                  | FCC-hh                                  |
|           | $\mathcal{L} = 450 \text{ fb}^{-1}$         | $\mathcal{L} = 3\,000 \text{ fb}^{-1}$ | $\mathcal{L} = 10\,000 \text{ fb}^{-1}$ | $\mathcal{L} = 30\,000 \text{ fb}^{-1}$ |
| 1         | 56  | 376                                    | 1 252                                   | 3 756                                   |
| 2         | 68  | 457                                    | 1 523                                   | 4 568                                   |
| 3         | 71  | 476                                    | 1 587                                   | 4 760                                   |

TABLE IV: The number of expected events related to  $H_0 \rightarrow \gamma Z$  decay.

| $f$ [TeV] | Number of expected events at the colliders: |  |   |   |
|-----------|---|--|---|---|
|           | LHC   | HL-LHC                                 | HE-LHC                                  | FCC-hh                                  |
|           | $\mathcal{L} = 450 \text{ fb}^{-1}$         | $\mathcal{L} = 3\,000 \text{ fb}^{-1}$ | $\mathcal{L} = 10\,000 \text{ fb}^{-1}$ | $\mathcal{L} = 30\,000 \text{ fb}^{-1}$ |
| 1         | 30  | 202                                    | 672                                     | 2 017                                   |
| 2         | 33  | 220                                    | 732                                     | 2 195                                   |
| 3         | 34  | 224                                    | 746                                     | 2 238                                   |

## V. CONCLUSIONS

In this work, we perform a phenomenological study of the production of the heavy Higgs boson  $H_0$  via gluon fusion in the context of the BLHM. Specifically, we analyze the one-loop decays of the  $H_0$  Higgs, which refer to  $H_0 \rightarrow gg, \gamma\gamma, \gamma Z$  processes. For these decays, the effects induced by the new particles of the BLHM and the particles of the SM are considered. As the BLHM has two independent energy scales,  $f$  and  $F$ , these represent the scales of the new physics of the model. In this way, we have generated phenomenological results for the branching ratios and production cross-sections of the  $H_0$  Higgs in analysis regions corresponding to  $f = [1000, 3000]$  GeV and  $F = [3000, 6000]$  GeV. For the considered intervals of the scales  $f$  and  $F$ , we analyzed the dependence of  $\text{Br}(H_0 \rightarrow X)$  on the aforementioned scales and found that the branching ratio shows sensitivity to variations in the  $f$  scale, this effect is not observed with the  $F$  scale. In the two study scenarios, the dominant branching ratios at the tree and one-loop level correspond to processes  $H_0 \rightarrow \bar{t}t$  and  $H_0 \rightarrow gg$  whose numerical predictions are of  $10^{-1}$  and  $10^{-2}$ , respectively. A rough estimate of the production cross-section of  $H_0$  was also implemented via gluon fusion. For this case, the numerical estimates of  $\sigma(gg \rightarrow H_0 \rightarrow Y)$  tell us that the  $H_0 \rightarrow gg$  process offers a very promising scenario for the search of the heavy particle  $H_0$  in future experiments such as LHC, HL-LHC, HE-LHC, and FCC-hh. In this approach, we have that for  $m_{H_0} \approx 1000$  GeV and  $f = 1$  TeV we could estimate around 11 453 events at the LHC, 76 355 events at the HL-LHC, 254 516 events at the HE-LHC and 763 548 events for the FCC-hh, which is a very optimistic scenario for the study of the scalar  $H_0$  predicted by the BLHM.

## Acknowledgements

E. C. A. appreciates the post-doctoral stay. A. G. R. and D. E. G. thank SNII (México).

- 
- [1] M. Schmaltz, D. Stolarski and J. Thaler, *JHEP* **09**, 018 (2010).
  - [2] S. Godfrey, T. Gregoire, P. Kalyniak, T. A. W. Martin and K. Moats, *JHEP* **04**, 032 (2012).
  - [3] P. Kalyniak, T. Martin and K. Moats, *Phys. Rev. D* **91**, 013010 (2015).
  - [4] T. Cisneros-Pérez, M. A. Hernández-Ruíz, A. Gutiérrez-Rodríguez and E. Cruz-Albaro, *Eur. Phys. J. C* **83**, 1093 (2023).
  - [5] E. Cruz-Albaro, A. Gutierrez-Rodriguez, M. A. Hernandez-Ruiz and T. Cisneros-Perez, *Eur. Phys. J. Plus* **138**, 506 (2023).
  - [6] E. Cruz-Albaro, A. Gutiérrez-Rodríguez, J. I. Aranda and F. Ramírez-Zavaleta, *Eur. Phys. J. C* **82**, 1095 (2022).
  - [7] E. Cruz-Albaro and A. Gutiérrez-Rodríguez, *Eur. Phys. J. Plus* **137**, 1295 (2022).
  - [8] N. Arkani-Hamed, A. G. Cohen, E. Katz and A. E. Nelson, *JHEP* **07**, 034 (2002).
  - [9] S. Chang, *JHEP* **12**, 057 (2003).
  - [10] T. Han, H. E. Logan, B. McElrath and L. T. Wang, *Phys. Rev. D* **67**, 095004 (2003).
  - [11] S. Chang and J. G. Wacker, *Phys. Rev. D* **69**, 035002 (2004).
  - [12] M. Schmaltz, *JHEP* **08**, 056 (2004).
  - [13] M. Schmaltz and J. Thaler, *JHEP* **03**, 137 (2009).
  - [14] X. F. Han, L. Wang, J. M. Yang and J. Zhu, *Phys. Rev. D* **87**, 055004 (2013).
  - [15] J. Reuter and M. Tonini, *JHEP* **02**, 077 (2013).
  - [16] C. Csaki, J. Hubisz, G. D. Kribs, P. Meade and J. Terning, *Phys. Rev. D* **67**, 115002 (2003).
  - [17] A. Abada *et al.* (FCC Collaboration), *Eur. Phys. J. ST* **228**, 755 (2019).
  - [18] ATLAS Collaboration, *Combined measurements of Higgs boson production and decay using up to 80 fb<sup>-1</sup> of proton-proton collision data at  $\sqrt{s} = 13$  TeV collected with the ATLAS experiment*, ATLAS-CONF-2019-005.
  - [19] D. Eriksson, J. Rathsman and O. Stal, *Comput. Phys. Commun.* **181**, 189 (2010).
  - [20] K. P. Moats, *Phenomenology of Little Higgs models at the Large Hadron Collider*, doi:10.22215/etd/2012-09748.
  - [21] T. A. W. Martin, *Examining extra neutral gauge bosons in non-universal models and exploring the phenomenology of the Bestest Little Higgs model at the LHC*, doi:10.22215/etd/2012-09697.
  - [22] S. P. Martin, *Adv. Ser. Direct. High Energy Phys.* **18**, 1 (1998).

- [23] G. Aad *et al.* (ATLAS Collaboration), *Phys. Lett. B* **809**, 135754 (2020).
- [24] A. Tumasyan *et al.* (CMS Collaboration), *JHEP* **05**, 233 (2023).
- [25] A. M. Sirunyan *et al.* (CMS Collaboration), *Phys. Lett. B* **805**, 135425 (2020).
- [26] A. Gutiérrez-Rodríguez, E. Cruz-Albaro and D. Espinosa-Gómez, *Feynman rules for Scalars at the Bestest Little Higgs Model*, arXiv:2312.08560 [hep-ph].
- [27] J. I. Aranda, T. Cisneros-Pérez, E. Cruz-Albaro, J. Montaña-Domínguez and F. Ramírez-Zavaleta, *Chromomagnetic dipole moment of the top quark in the Bestest Little Higgs model*, arXiv:2111.03180 [hep-ph].
- [28] R. L. Workman *et al.* (Particle Data Group), *Prog. Theor. Exp. Phys.* **2022**, 083C01 (2022).
- [29] E. Barradas, J. L. Diaz-Cruz, A. Gutierrez and A. Rosado, *Phys. Rev. D* **53**, 1678 (1996).
- [30] A. Denner and S. Dittmaier, *Nucl. Phys. B* **734**, 62 (2006).
- [31] W. Altmannshofer and D. M. Straub, *JHEP* **09**, 078 (2010).
- [32] R. L. Workman *et al.* (Particle Data Group), *Prog. Theor. Exp. Phys.* **2022**, 083C01 (2022).
- [33] G. Aad, *et al.* (ATLAS Collaboration), *Eur. Phys. J. C* **81**, 396 (2021).
- [34] A. Abada *et al.* (FCC Collaboration), *Eur. Phys. J. ST* **228**, 1109 (2019).
- [35] CERN, 2022. <https://hilumilhc.web.cern.ch/article/l3-schedule-change>
- [36] A. Abada *et al.* (FCC Collaboration), *Eur. Phys. J. C* **79**, 474 (2019).
- [37] W. Barletta, M. Battaglia, M. Klute, M. Mangano, S. Prestemon, L. Rossi and P. Skands, *Nucl. Instrum. Meth. A* **764**, 352 (2014).